metals

MDPI

Article

Study of Micro Structural Material Changes after WEDM Based on TEM Lamella Analysis

Katerina Mouralova [1], Radim Zahradnicek [2], Libor Benes [3], Tomas Prokes [1,*], Radim Hrdy [2] and Jiri Fries [4]

1 Faculty of Mechanical Engineering, Brno University of Technology, 61669 Brno, Czech Republic; mouralova@fme.vutbr.cz
2 Faculty of Electrical Engineering and Communication, Brno University of Technology, 61669 Brno, Czech Republic; zahradnicek@vutbr.cz (R.Z.); hrdy@feec.vutbr.cz (R.H.)
3 Faculty of Production Technologies and Management, Jan Evangelista Purkyně University, 40096 Ústí nad Labem, Czech Republic; libor.benes@ujep.cz
4 Department of Production machines and design, Technical University of Ostrava, 70833 Ostrava, Czech Republic; jiri.fries@vsb.cz
* Correspondence: tomas.prokes@vutbr.cz; Tel.: +42-0739-96-8492

Received: 23 June 2020; Accepted: 11 July 2020; Published: 14 July 2020

Abstract: Wire electrical discharge machining is an unconventional machining technology that is crucial in many industries. The surface quality of the machined parts is carefully monitored, but the condition of the subsurface layer also plays a crucial role, especially in case of defects occurrence such as cracks or burnt cavities. The subsurface layer of individual materials is affected differently due to wire electrical discharge machining. For this reason, this study was carried out focusing on a detailed analysis of transmission electron microscope (TEM) lamella made of Ti-6Al-4V titanium alloy, AlZn6Mg2Cu aluminum alloy, pure molybdenum, Creusabro 4800 steel, and Hardox 400 steel. The attention was first of all paid to the concentration and distribution of individual elements in the recast layer and also in the base material, which was often affected by wire electrical discharge machining. Further, a diffraction analysis was performed for each TEM lamella in the adhesive area and in the base material area. In order to assess the macro-effects on the machined material, the topography analysis of the machined surfaces and the morphology analysis were performed using electron microscopy.

Keywords: wire electrical discharge machining (WEDM); electrical discharge machining; microstructure; transmission electron microscope (TEM) lamella; recast layer; topography; morphology

1. Introduction

In spite of its increased energy intensity, the unconventional technology wire electrical discharge machining (WEDM) is very efficient for machining conventionally hard to machine materials such as titanium, aluminum and nickel alloys, pure metals or high hardness steels. Due to the fact that there are no demands on the mechanical properties of a machined material during machining, only on its electrical conductivity, the utilization of this technological process is almost unlimited for newly emerging super alloys. It finds its application in many manufacturing sectors, especially in the automotive, aerospace, medical, and military industries, where WEDM has become an indispensable technological operation [1].

The principle of WEDM is the division of material by means of a thermoelectric phenomenon, whereby periodically repeating electrical impulses lead to the erosion of the machined material and at the same time to its evaporation. The tool usually consists of a brass wire with diameters of 0.3 up

to 0.02 mm, which never touches the workpiece. That, therefore, enables manufacturing thin-walled profiles that are not subjected to mechanical forces, as in conventional machining [2].

Due to the very high temperatures 10,000–20,000 °C [3] incurred during the WEDM, the surface layer, the so-called recast layer, is completely melted at the cut point and then very quickly cooled by the dielectric fluid flow. As a result, it is transformed and very distinctive microstructural differences from the base material occur. The recast layer thickness and its multiple occurrence on the workpiece surface are determined by many different factors. It is primarily a mechanical and physical property set of the machined material, but also parameters of the machine setting, the number of cuts made, etc. [4].

Klink [5] in the study about the WEDM dressing and truing of diamond grinding wheels, fine grained metal bonded, also focused on the examination of the damage of a thermal grit surface and the graphitization of diamond. For the investigation of the amount of the graphitization, a crystallographic analysis was employed. To carry out this analysis a tiny electron transmission microscope (TEM)-lamella was produced of one eroded surface diamond grit by the focused ion beam (FIB). This helped reveal three carbon layers under two preparation layers, the inner layer crystalline structure and the outer layers amorphous structures, which indicated graphitization. Huang et al. [6] researched the microstructure analysis of the steel surface of the martensitic stainless fine-cut by WEDM. During the experiments, they focused on the analysis of the TEM-microstructure of finished surfaces as well. To carry it out, cross-section and plain-view TEM-samples were produced. For their preparation, the ion milling and dimpling processes were employed to make a small hole in the center of the disc sample, which enabled examining the microstructures with the help of TEM and energy-dispersive X-ray spectroscopy (EDX). Moreover, from the output of the TEM study, a heat-affected zone, specified as the white layer, was found in the surface layer, and a few spherical deposits were also registered. Klocke et al. [7] studied the white layer structure and composition in the WEDM process. To analyze the white layer metallurgical structure a thinFIB-lamella was produced utilizing the FIB technic. Meanwhile, TEM characterizations were performed, and the energy-filtered TEM images were obtained using a Gatan GIF system. While analyzing the carbon and recast layers, the FIB-lamella becomes thinner from the left to the right. The thin lamella outputs in an improved quality of the image, and subsequently a comprehensive analysis was carried out in the lamella's very right part. Zhang [8] focused on the impact of WEDM parameters on the integrity of the surface of nanocomposite ceramics, where he studied the microstructure. A TEM micrograph analysis was employed in the study, which displayed the fine-grained microstructure of the TiN/Si_3N_4 composite and TiN particles were allocated throughout Si_3N_4 matrices. It was also evident, that surfaces of Si3N4 particles were fully coated by TiN particles. Huang et al. [9] investigated the rough-cut surface characteristics of tempered and quenched martensitic stainless employing WEDM. The TEM examination was done using the cross sectioned samples obtained from the samples tempered at 600 °C and with appropriate mechanical properties (strength, toughness, and hardness). With the help of these TEM specimens, an amorphous layer was detected on a few parts of the furthermost surface of the cut with randomly distributed fine crystalline particles inside it. While the examination of the recast layer, spherical electrode deposits, and a lot of one of the deposits of the wire-electrode material at the gas void side were detected in it, which were evident on the dark- and bright-field TEM micrographs. Murray et al. [10] was interested in the TEM analysis on the WEDM surface of a single-crystal silicon. For the experiments, focused ion beam machining was carried out to produce a lamellar out of one of the machined holes. Since it was impossible to make a lift out from the whole bottom surface because of the entry angle of a manipulator, an "L" shaped lamellar was produced from the top edge of the hole. Jose and Shunmugam [11] investigated the white layer built on the WEDM Ti6Al4V surface due to the surface quality and the component life. It was found, that the phases detected in the white layer are organized in the microstructure of the fine lamellar. The microstructure of the lamellar was formed as an output of plain cooling from the above β transus temperature. The amorphous phase was detected because of the oxygen high affinity in the microstructure of higher cooling rates and the fine lamellar in the WEDM process. Moreover, the rise in hardness was found because of the grain structure of a very fine lamellar

detected in the white layer. Liu et al. [12] studied crystallography, compositions, and characteristics of the white layer by the WEDM of a nitinol shape memory alloy. For the TEM analysis, the EDM specimens at the main cut were selected due to the ability of the main cut to produce a thick white layer. For the preparation of the electron transparent TEM specimen, a variation of the FIB in situ lift-out method was utilized for TEM foil producing. Throughout the study, the TEM analysis was employed to examine the white layer microstructure and crystallography and heat affected zone by the WEDM of Nitinol. Sanchez [13] presented computer simulation software for the analysis of error in wire electrical discharge machining of taper-cutting. Punturat [14] in his study focused on influence of major process parameters on the cut surface characteristics in the wire electrical machining of silicon. Chaudhari [15] in his work investigated the surface integrity of WEDM-processed nitinol samples.

Since the recast layer affects the wear, fatigue, and corrosion of the electro-erosion machined parts, it is necessary to study this phenomenon in detail, since understanding it can lead to an increase in the lifetime of the manufactured parts. There are several studies dealing with these microstructure changes in the recast layer, but only for a few materials, with no complex comparison of mechanically and physically different materials. Therefore, in order to make a detailed and comprehensive comparison of alloys, pure metal, and hard-to-machine steels, this extensive study was aimed at mapping the microstructural changes in the recast layer and its boundary with the base material.

2. Experimental Setup and Material

2.1. Experimental Material

Samples for the study were produced of the AlZn6MgCu aluminum alloy, Ti-6Al-4V titanium alloy, pure molybdenum, Creusabro 4800 steel, and Hardox 400 steel, with the chemical composition of the materials and their properties summarized in Table 1, and their microstructure was shown in Figure 1. The individual materials were chosen so that the differences in mechanical properties were as large as possible and the effects of machining on completely different materials could be monitored. A 15 mm thick workpiece was utilized for all specimens. Subsequently, all samples were reduced to a shape ideal for the electron microscope used. The TEM lamellas are located in the center of each sample on the top surface of Figure 1f.This area is original after being cut from the workpiece before reducing the sample. None of the materials was heat treated.

Table 1. Properties of individual materials used for sample production (all the information is based on the individual material sheets that were supplied in a paper form together with the materials).

Properties					
Material	**R_m (MPa)**	**$R_p0.2$ (MPa)**	**Hardness**	**Thermal Conductivity ($W \cdot m^{-1} \cdot K^{-1}$)**	**Electrical Resistivity ($\Omega \cdot m$)**
AlZn6Mg2Cu	550	485	145 HB	237	$2.7 \cdot \times 10^{-8}$
Ti-6Al-4V	800	700	334 HB	6.7	0.178
Molybdenum	630	550	220 HV	138	5×10^{-8}
Creusabro	1200	900	370 HB	54	1.38×10^{-9}
Hardox	1250	1000	400 HB	54	$1.38 \times \cdot 10^{-9}$
Chemical Composition (wt%):					
AlZn6Mg2Cu	2.5% Mg, 6% Zn, 1.9% Cu, Al–balance				
Ti-6Al-4V	4% V, 6% Al, max 0.2% O, max 0.25% Fe,Ti–balance				
Molybdenum	99.999% Mo				
Creusabro	1.6% Mn, 1.9% Cr, 0.2% C, 0.2% Ni, 0.4% Mo, 0.2% Ti, max 0.018% P, max 0.005% S, Fe–balance				
Hardox	0.7% Si, 0.3% C, 1.6% Mn, 1.5% Ni, 0.6% Mo, 1.4% Cr, max 0.025% P, max 0.01% S, Fe–balance				
Application:					
AlZn6Mg2Cu	High-stressed structures working long-term up to 100–120 °C, airspace industry-covers, longitudinal ribs, reinforcements and partitions.				
Ti-6Al-4V	Aircraft and weapon components, medical implants, turbine blades, sports equipment and chemical process equipment.				
Molybdenum	In addition to physical applications, it is used in the chemical industry, in glassmaking, metallurgy for hot working tools, in the electronics and electrical engineering industries.				
Creusabro	In quarries and mines, in cement and steel industry, agricultural and foundry technology.				
Hardox	Truck body design, crushers, containers, scrap metal processing machines, gears, conveyors, and cutting knives.				

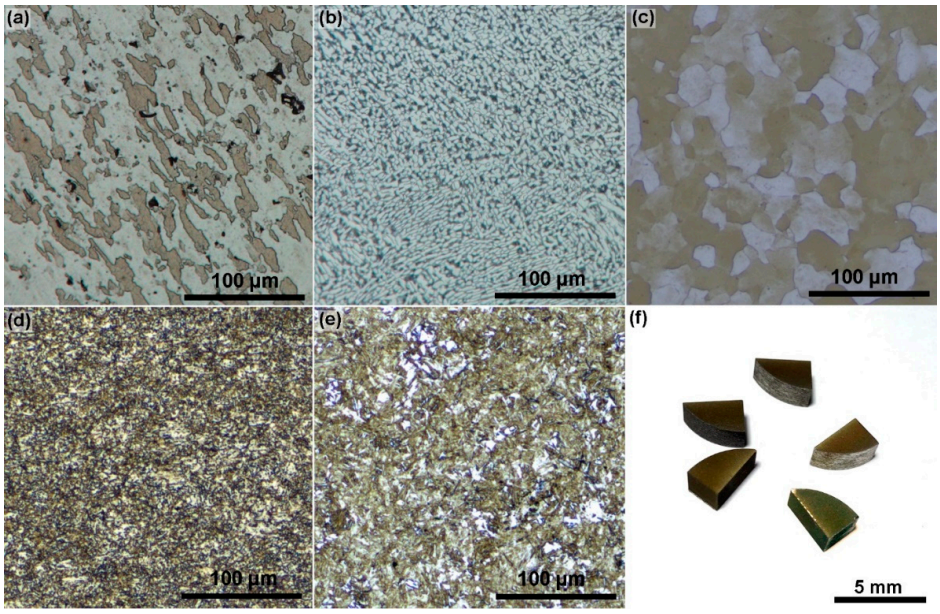

Figure 1. Microstructures of materials used for specimens, optical images, (**a**) AlZn6Mg2Cu aluminum alloy-etched with Keller's reagent, (**b**) Ti-6Al-4V titanium alloy-etched with Keller's reagent, (**c**) pure myolybdenum-etched with Hasson etchant, (**d**) Creusabro 4800-etched with Nital, (**e**) Hardox 400-etched with Nital, (**f**) machined samples.

In order to be able to study the microstructure of individual examined materials, metallographic preparations were created, which were made using common techniques with the equipment from STRUERS (polishing with diamond pastes and wet grinding utilizing Tegramin 30–the automatic preparation system from STRUERS, the final mechanical-chemical polishing was done with the OP-Chem suspension from STRUERS). Furthermore, the microstructure was imaged using an Axio Z1m light microscope (LM) (ZEISS, Jena, Germany)from the manufacturer ZEISS.

2.2. WEDM Machine Setup

For the machining, an Axio Z1m light microscope (LM) (ZEISS, Jena, Germany))from Makino, which has a dielectric bath in which the workpiece is completely immersed, was used. The brass wire CUT E with a diameter of 0.25 mm supplied by Penta, was employed as the tool electrode. The cutting process parameters, such as pulse on/off time, discharge current, and wire speed have been set based on the setting recommended by the manufacturer for each material (Table 2). This setting for each parameter was identified on the basis of the multiple previous tests and also on the recommendation of the machine manufacturer.

Table 2. Machine setup parameters values.

Material	Wire Speed	Gap Voltage	Discharge Current	Pulse on Time	Pulse off Time
	($m \cdot min^{-1}$)	(V)	(A)	(µs)	(µs)
AlZn6Mg2Cu	10	70	35	10	40
Ti-6Al-4V	10	70	35	10	30
Pure molybdenum	10	70	35	6	30
Creusabro 4800	12	60	25	8	40
Hardox 400	14	70	35	6	30

2.3. Production of TEM Lamella

The production of the individual lamella was performed using a scanning electron microscope (SEM) (FEI, Hillsboro, OR, USA) of the Helios type from the manufacturer Thermo Fisher Scientific. The production of lamellas is an extensive process in which a protective layer is applied to the upper

part of the newly formed lamella, which is usually 2.2 µm thick and consists first of platinum and then of carbon. Then, the production of the lamella itself is carried out using FIB, when a trench measuring 12 × 20 × 24 µm is created around the lamella. Under the tilt, the lamella is then cut from the base material and transferred to a copper holder. In this holder, the lamella is finalized and its final thinning reaches the required thickness of 0.2 µm, which allows the observation in TEM. Figure 2 shows the whole process of the lamella production. There is also a TEM image of the entire lamella. The transmission electron microscope was manufactured by Thermo Fisher Scientific and its type marking is Titan.

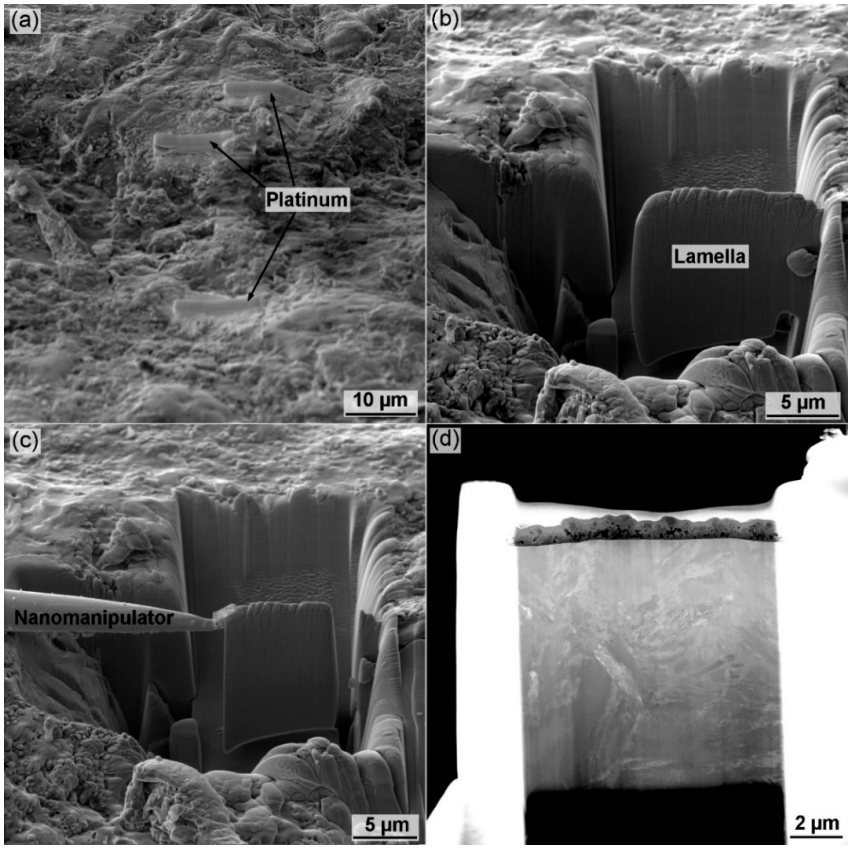

Figure 2. Preparation of transmission electron microscope (TEM) lamella (**a**) platinum deposition by Electron-beam-induced deposition (EBID) and focused ion beam induced deposition (FIBID) (SEM), (**b**) digging of the tripartite trench and cutting of the lamella by FIB (SEM), (**c**) extraction of the lamella by nanomanipulator (SEM), (**d**) final thinning of the lamella (TEM).

3. Results and Discussion

3.1. Experimental Methods

In order for the manufactured samples to be observed in SEM, they had to be thoroughly cleaned in an ultrasonic cleaner Emmi-12 HC (Emag, Ann Arbor, MI, USA). They were further analyzed and studied in SEM LYRA3 from Tescan, which was equipped with an EDX detector from Bruker (Tescan, Brno, Czech Republic). The topography of machined surfaces was studied using a Talysurf CCI Lite non-contact 3D profilometer from Taylor Hobson (Taylor Hobson, Leicester, UK)

3.2. Surface Topography Analysis

The topography of the functional surface affects the reliability of the component and the service life. The topography depends on the running-in time, wear resistance, accuracy of machine parts and their noise, friction losses, electrical resistance, heat transfer, etc. Therefore, the topography affects the course

of the physical and chemical phenomena that accompany the operational activity of the functional surface of the part. The evaluation and use of topography to increase the efficiency of machine parts and their quality is one of the basic reasons for its detailed study. Due to the abovementioned reasons, not only profile parameters (Ra, Rq, Rz) but also basic profile parameters (Pa, Pq, Pz) and area parameters (Sa, Sq, Sz) were evaluated [16]. All parameters were assessed employing a non-contact 3D profilometer Talysurf CCI Lite to the corresponding standards for the area parameters ISO 25178-2 [17] and profile parameters ISO 4288 [18] standard. All parameters were assessed on 1024 profiles gotten from S-F surfaces made with the 20x objective. Five random places on each workpiece were chosen for the measurement and an average of these values was subsequently calculated.

The evaluated values of individual surface topography parameters were used in the graph in Figure 3. The lowest values and thus the highest surface quality was achieved when machining pure molybdenum, namely Ra 1.86 µm. On the other hand, the lowest machined surface quality was in the case of Hardox 400 steel (Ra 3.5 µm).If we compare these results with the Ikram et al. [19] or Majumder and Maity [20] studies for the machining of Nitinol, it is clear that it was possible to achieve lower Ra (Ra 2.41 µm) parameters in the machining of non-ferrous metals than in the machining of steels.

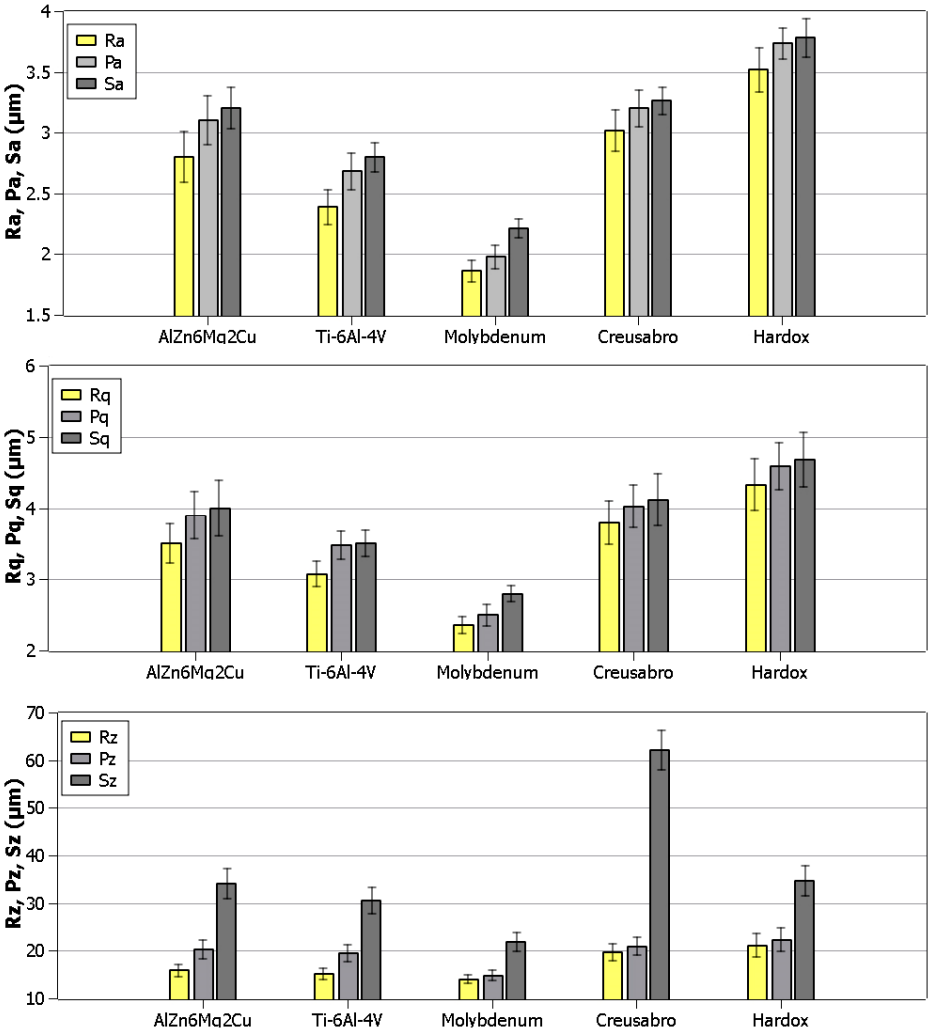

Figure 3. The assessed parameters of the basic profile (average height of profile (Pa), mean peak to valley height of primary profile (Pz), and root mean square height of profile (Pq)), area (arithmetical mean height (Sa), maximum surface height (Sz), and root mean square height (Sq)),and profile parameters (arithmetical mean deviation of profile (Ra), maximum height of profile (Rz), and root mean square deviation (Rq)) of different experimental specimens.

3.3. Analysis of Surface Morphology

In the course of WEDM, a very specific morphology is created due to the influence of electrical impulses, which is made by a big quantity of individual craters, which were formed by melting and washing away small particles of the material. The different appearance of the morphology is an absolutely typical feature of this type of unconventional technology. This is influenced not only by the mechanical and physical properties of the machined materials, as it was found out in Mouralova's publication [21], but also by different heat treatments or setting of machine parameters, which was published in Mouralova's study [22]. Another factor that plays a significant role in the appearance of morphology in this machining process is the direction of the orientation of the section through the semi-finished product, which was published in Mouralova's study [23].

All the machined samples surface morphology was studied by electron microscopy. Secondary electrons (SE) were used for displaying in all the cases, and the samples were always studied at 1000, 2500×, and then 4000× magnification. None of the materials was heat treated and all the samples were cut in the same orientation through semi-product.

Figure 4 shows the morphologies of all machined materials, showing their great diversity. The size of the craters as well as their shape, frequency, and the amount of completely melted and recooled material are different. Cracks and other subsurface defects are a very extensive problem in the tested materials. It was therefore solved in detail and tested in individual impacted articles for each material separately. This is mainly due to finding the optimum setting of machining parameters or the orientation of cut through semi-product, in which defects do not occur or to a limited extent.

3.4. The analysis of AlZn6Mg2Cu Aluminium Alloy TEM Lamella

The analysis of the aluminium alloy lamella in TEM included the determination of the local chemical concentration of elements in the workpiece (Figure 5 and Table 3) and the study of the crystal lattice change affected by machining. The observations were made at a300 kV acceleration voltage. The beam current utilized during the EDX measurement was set to 1 nA and was run in a scanning mode. At this setting, the electron beam size was 0.5 angstrom. The emergence of a recast layer is very typical for this kind of unconventional machining. It is a layer that has been completely melted and very quickly cooled by a dielectric fluid flow by the action of a plasma channel of up to 20,000 °C [3] during individual discharges. Due to the material match of the electrode elements and elements in the aluminium alloy, it is not possible to determine unequivocally where the increased concentration of copper and zinc originates from in the recast layer. Furthermore, copper precipitates in the grain boundary area were discovered in the lamella image.

The study of the influence of the crystalline lattice of the base material was carried out in a diffraction mode, as shown in Figure 5. The measurement in this case was carried out unlike EDX in the transmission mode. The trace size was 100 nm and the beam current was up to 14 nA. The high beam current increases the brightness of the individual diffraction points. By reducing the trace of the electron beam, a similar effect can be achieved at lower currents. The comparison of the diffraction image of the base material with the recast layer area shows that there was a slight increase in the residual stress in the layer, resulting in a change in the distance of the individual points. In addition, points corresponding to another crystal plane appeared. A similar result in WEDM was found for other materials. For example, Liu [12] noted a similar change in crystal lattice after WEDM machining on the nitinol material.

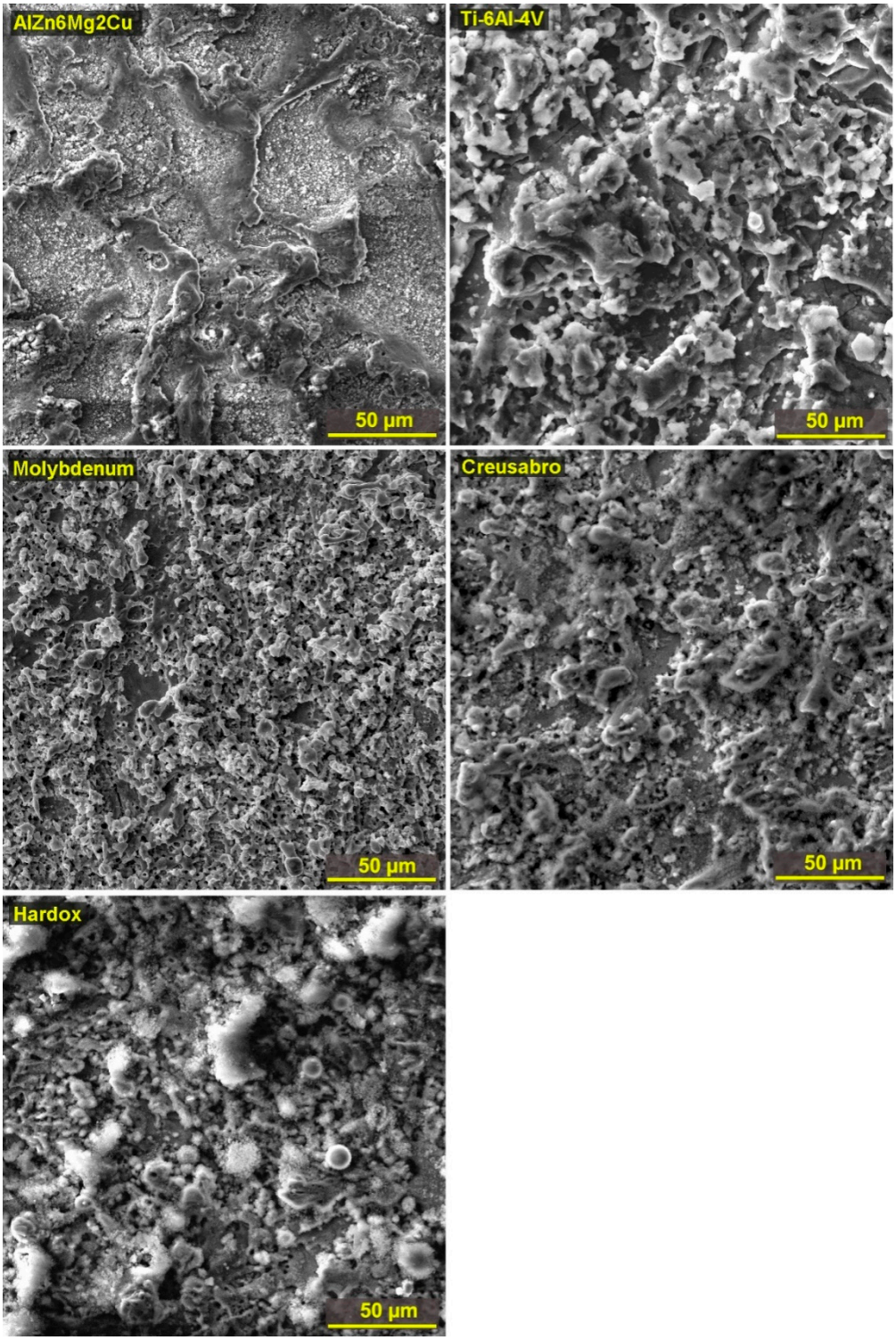

Figure 4. The surface morphology of SEM (Secondary electrons: SE) specimens, magnified at 1000×.

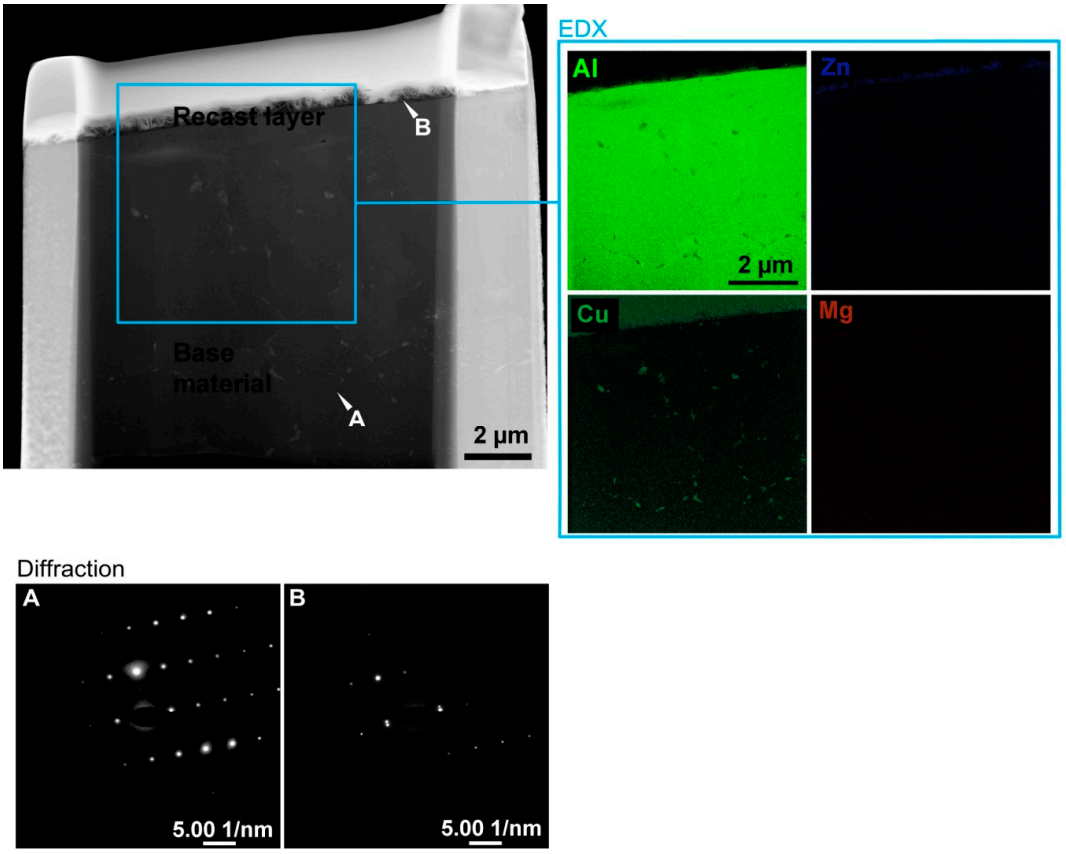

Figure 5. TEM lamella of the AlZn6Mg2Cu aluminium alloy including the map of the arrangement of separate elements in the examined area of the lamella and a comparison of the diffraction pattern of A—base material and with B—the area near the recast layer.

Table 3. The chemical composition analysis in eachEDX detail according to Figure 5.

Element	Atomic Fraction (%)	Fit Error (%)
Mg	3.09	0.88
Al	88.69	30.75
Cu	6.09	1.92
Zn	2.13	0.67

3.5. The analysis of Ti-6Al-4V Titanium Alloy TEM Lamella

Due to the total size of the lamella made of titanium alloy, two EDX measurements were performed in the scanning mode at 300 kV with the beam current of 1 nA. The first measurement was focused on the upper half with the recast layer and the second on the base material, as shown in Figure 6. From the EDX measurement (Table 4) of the first half of the lamella, it was clear that during the machining process there was a strong diffusion of the electrode material (copper and zinc) into the machined material. The higher copper concentration can be explained by the higher copper solubility in titanium than zinc. In addition, increased concentrations of aluminum, iron, and oxygen have been monitored in the recast layer. The presence of oxygen in the adhesive material correlated with the presence of zinc, which can be justified by the reaction of zinc with the oxygen contained in the base material. Mixing of the base material with the electrode is often observed in the case of WEDM machining due to the nature of this method. The same machining effect was observed, for example, in the case of TiN/Si_3N_4 ceramics, where the electrode material was also mixed with the base material as detected by EDX Zhang [8].

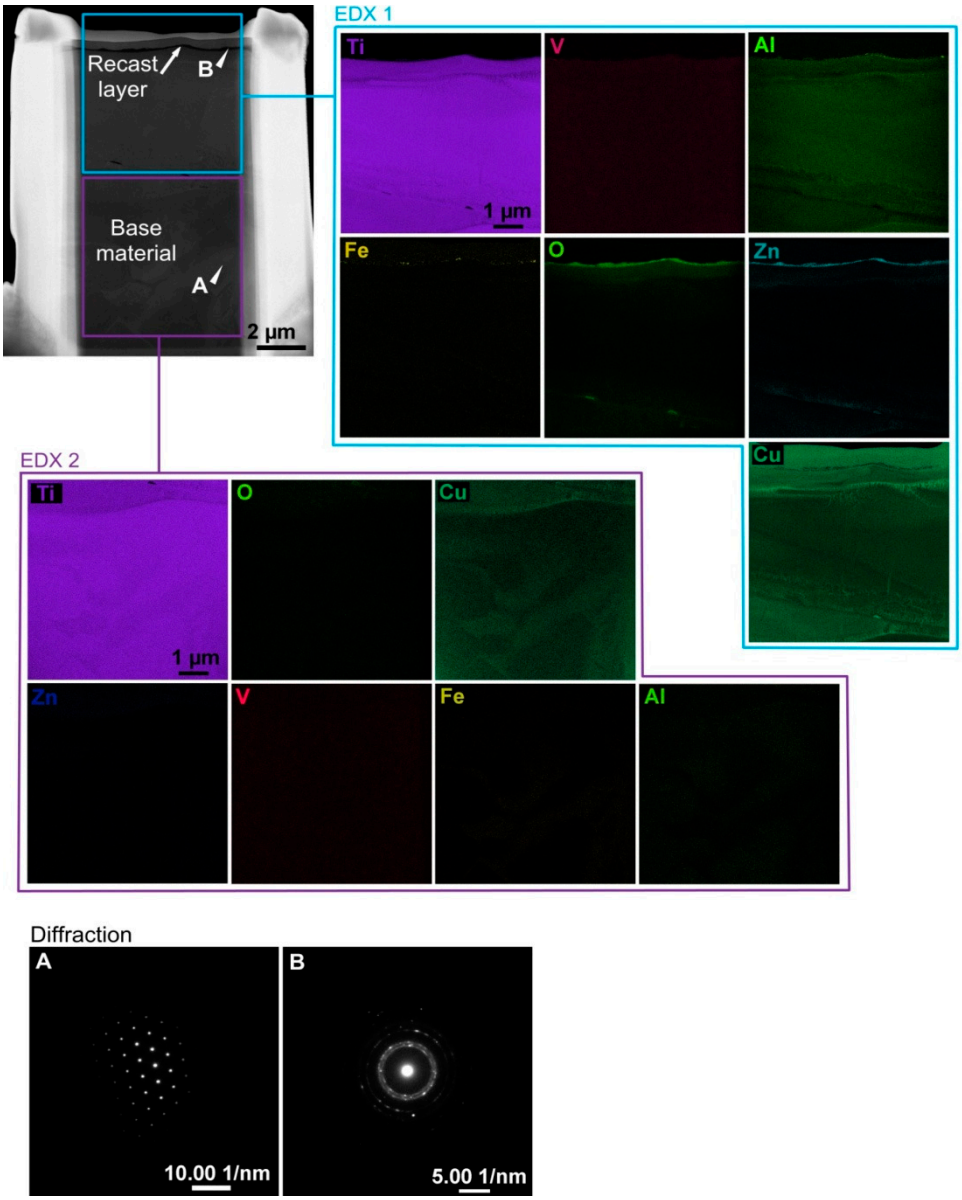

Figure 6. TEM lamella of Ti-6Al-4V titanium alloy including the map of distribution of separate elements in the examined area of the lamella and a comparison of the diffraction pattern of A—base material and with B—the area near the recast layer.

Table 4. The chemical composition analysis in each detail according to Figure 6.

Element	Detail 1		Detail 2	
	Atomic Fraction (%)	Fit Error (%)	Atomic Fraction (%)	Fit Error (%)
O	6.91	1.22	4.03	0.75
Al	5.91	1.56	6.15	1.65
Ti	72.87	16.02	76.14	17.06
V	0.00	0.01	0.00	0.00
Fe	0.39	0.08	0.49	0.11
Cu	13.21	2.91	12.98	2.91
Zn	0.72	0.16	0.21	0.05

The EDX measurement of the lower part of the lamella showed an equal arrangement of the elements of the base material except for iron, as shown in Figure 6. The appearanceof copper and zinc on the entire surface studied can be explained by the secondary material transfer from the recast

layer by FIB. The transfer occurred due to the large difference in density between the base material and the recast layer. One of the ways to prevent the secondary transfer is the final polishing of the lamella by a focused ion beam with the accelerating voltage of only 5 instead of 30 kV with the current of 40 pA. With this low voltage and a ± 7 degrees angle change, an effective reduction of secondary contamination can be achieved. The observation of the crystal structure of the base material and the recast layer interface was done in a diffraction mode, as shown in Figure 6. From the diffraction pattern comparison of the base material and the area near the adhesive, it was evident that the major amorphization of the crystal structure of the material occurred due to WEDM in the area of the adhesive. This change manifested itself in the diffraction pattern by changing from regularly spaced points in a circle with several separate light points. A similar effect was observed by other scientific groups dealing with the Ti-6Al-4V titanium alloy Jose and Shunmugam [11].

3.6. The Analysis of Pure Molybdenum TEM Lamella

The pure molybdenum lamella was examined for a local chemical composition and crystal lattice changes due to WEDM. In order to determine the total electrode contamination, an initial EDX measurement was performed in the scanning mode at 300 kV and a current of 1 nA, as shown in Figure 7 (Table 5), followed by a secondary measurement in the crack area. It may be noticed from the initial chemical composition of the lamella that the electrode material (copper and zinc) has diffused into the grain boundary area. The overall nature of the electrode material contamination is due to both the aforementioned diffusion and the secondary transfer due to the recast layer sputtering. This secondary contamination can be reduced by using a different approach to lamella production. When creating a lamella from a metallographically modified sample, it is possible to unambiguously determine the size of the base material and the recast layer. When producing a lamella from the surface of a machined sample, this cannot be achieved because the size of the base material and the recast layer is known only while polishing. In addition, the secondary contamination does not occur due to sputtering during the lamella thinning from the metallographic specimen. For example, this approach has been used in the preparation of a nitinol shape memory lamella Liu et al. [12]. From the second EDX measurement in the cracks area, it is evident that the electrode material has also diffused into these places, with copper being most notable. Filling of the crack with the electrode material probably occurred during the cooling of the material at the end of the WEDM process. The effect of the electrode material diffusion into the cracks caused by WEDM has also been monitored in the machining of stainless martensitic steel Huang et al. [9].

Table 5. The chemical composition analysis in each detail according to Figure 7.

Element	Detail 1		Detail 2	
	Atomic Fraction (%)	Fit Error (%)	Atomic Fraction (%)	Fit Error (%)
Cu	18.01	3.58	16.53	3.33
Zn	0.15	0.03	0.04	0.01
Mo	81.84	18.60	83.43	19.15

The material thinning in the crack area was due to different material compositions from the rest of the lamella. This difference led to faster sputtering of the material in the crack area than in other locations. The main difference between the materials is the ion sputtering coefficient. If the base material is sputtered with the same speed as the intermix material or faster, you will not see a crack formation due to lamella preparation. In the diffraction mode, the measurement of the impact of WEDM on the crystalline structure of the material was performed, as shown in Figure 7. From the diffraction pattern comparison of the base material of the lamella with the area near the adhesive, which was done in the transmission mode with a beam current of about 12 nA, it is evident that the residual stress increased in the material due to WEDM, which caused the change in the position of the individual diffraction points. The increase in residual stress due to WEDM was also monitored in

other materials. For instance, when processing a silicon single crystal, where it is very easy to observe any changes in the crystalline structure caused by mechanical machining or material impurities, due to the crystallography of the material Murrayet al. [10].

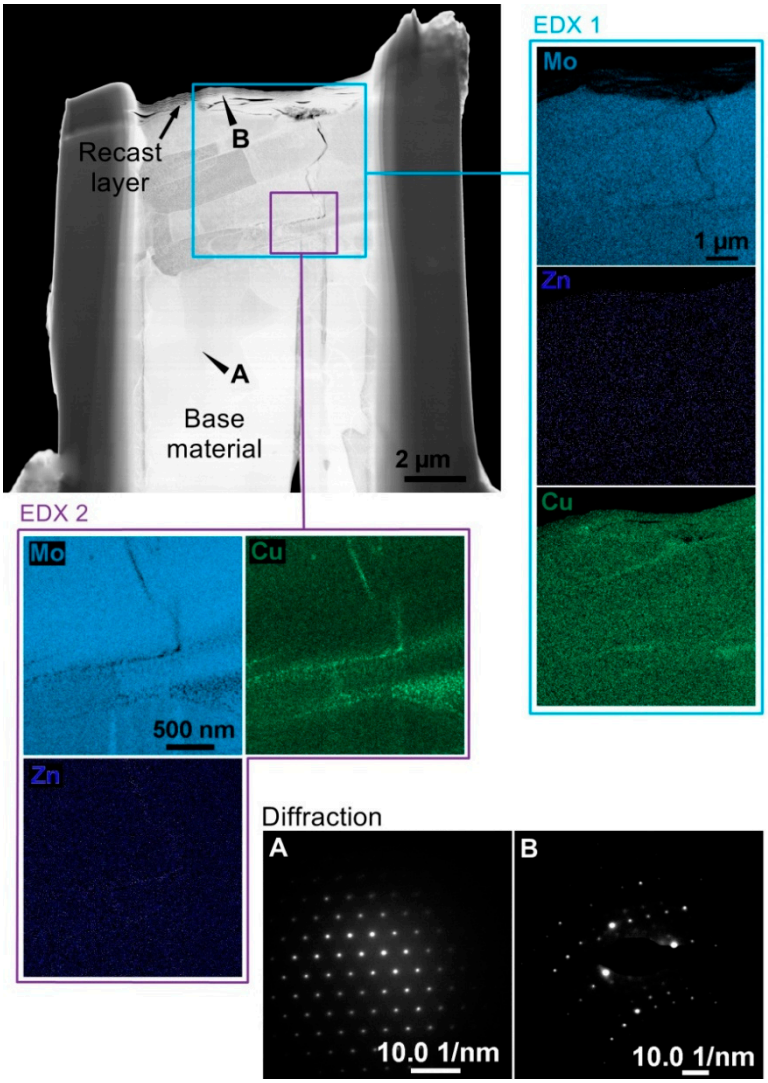

Figure 7. TEM lamella of pure molybdenum including the map of arrangement of separate elements in the examined area of the lamella and a comparison of the diffraction pattern of A—base material and with B—the area near the recast layer.

3.7. The Analysis of Creusabro 4800 TEM Lamella

Due to the size of the Creusabro 4800 steel lamella, two EDX measurements were performed in the scanning mode at 300 kV with a beam current of about 1 nA. The first measurement was focused on the composition of the adhesive, the second on the base material, both of which are shown in Figure 8 (Table 6). The increased concentration of some elements on the surface of the adhesive was detected from the EDX recast layer measurement. These were mainly carbon, phosphorus, sulphur, titanium, and zinc. In addition, the appearance of iron in the recast layer coincided with the appearance of other elements, such as Mn, Ni, Cr, Ti, and S. The material from the tool electrode (copper and zinc) was significantly present in the recast layer. The analysis of the base material showed an equal distribution of most alloying elements except for titanium, which in some places formed a separate grain, as shown in Figure 8 as EDX 2.

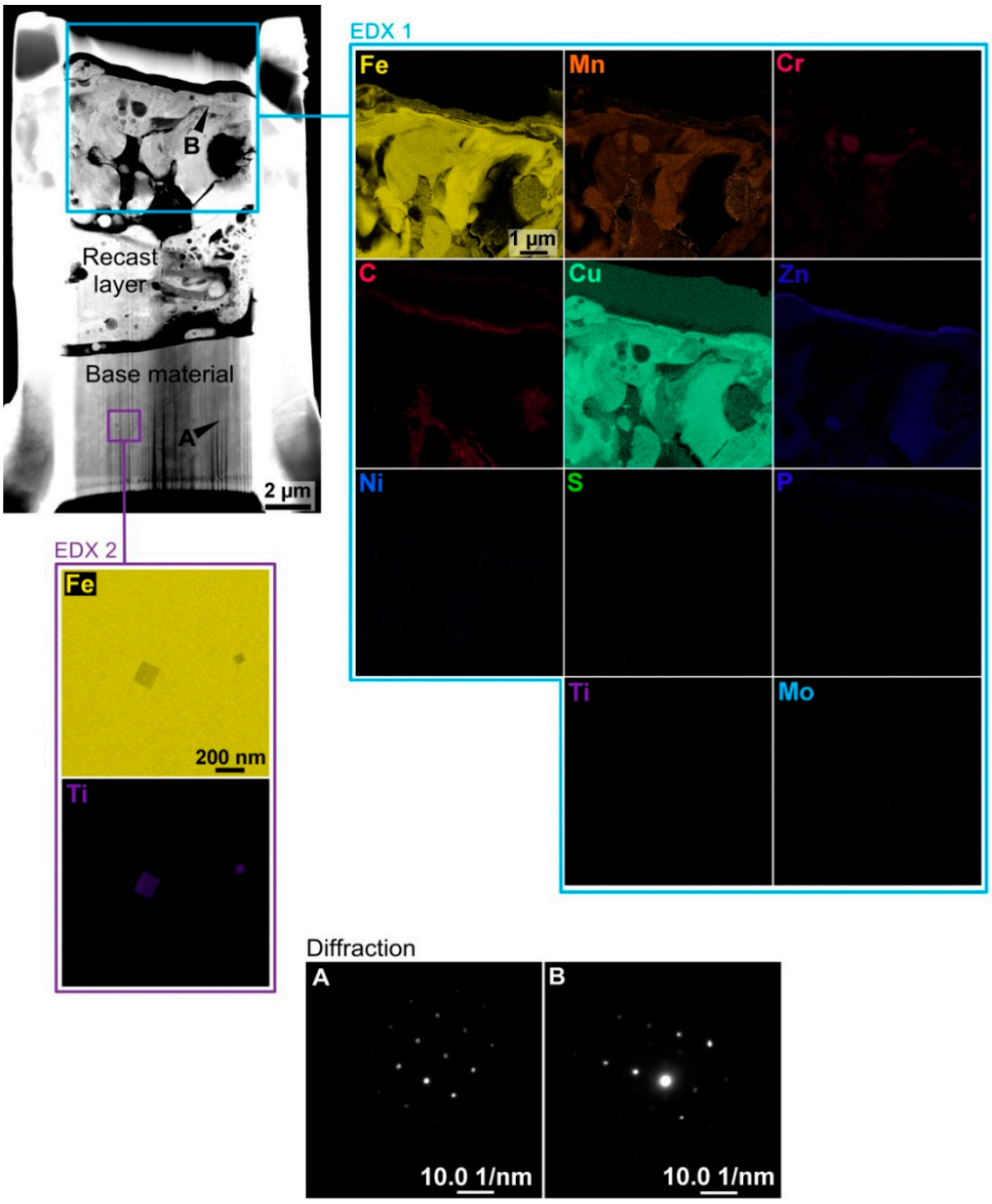

Figure 8. TEM lamella of Creusabro 4800 steel including the map of the arrangement of separate elements in the examined area of the lamella and a comparison of the diffraction pattern of A—base material and with B—the area near the recast layer.

In order to define the impact of WEDM on the crystal structure, a measurement in the diffraction mode was performed in the transmission mode at a current of about 11 nA. From the comparison of the diffraction patterns of the base material with the area near the adhesive, it is evident that due to the WEDM there was an increase in the residual stress, which caused a change in the position of the individual points, as shown in Figure 8. Similar effects on the crystal lattice by the WEDM method have been observed for other materials, for example Vanadium 4, which has been studied in Klocke et al. [7]. However, Klocke observed the change of crystal lattice on the image taken with the atomic resolution, where it was possible to study the rearrangement of individual atoms.

Table 6. The chemical composition analysis in eachdetail according to Figure 8.

Element	Detail 1		Detail 2	
	Atomic Fraction (%)	Fit Error (%)	Atomic Fraction (%)	Fit Error (%)
C	4.22	0.61	1.48	0.29
P	4.26	1.01	0.04	0.01
S	0.00	0.02	0.03	0.01
Ti	0.01	0.00	0.20	0.05
Cr	0.89	0.18	1.47	0.35
Mn	0.74	0.15	1.32	0.31
Fe	49.63	9.72	83.71	19.73
Ni	0.13	0.02	0.23	0.05
Cu	33.98	6.66	11.40	2.69
Zn	6.08	1.19	0.04	0.01
Mo	0.07	0.01	0.09	0.02

3.8. The Analysisof Hardox 400 TEM Lamella

With an accelerating voltage of 300 kV and a current in the beam of 1 nA, an analysis of the chemical composition of the Hardox lamella (Figure 9) was performed, which showed a homogeneous distribution of elements outside the recast layer. In this recast layer, there was a classic mixing of elements (Table 7) of the basic material and diffused elements from the tool electrode and also an increase in the local concentration of elements: Nickel, carbon, chromium, silicon, manganese, and molybdenum. The highest concentration of the elements was detected at the recast layer interface: Copper, silicon, and manganese. A small amount of copper was observed on the surface of the lamella, which was caused by the secondary transfer of material from the recast layer during dedusting. The contamination of the base material surface with the secondary transfer can also be reduced by changing the lamella orientation during the sputtering. In this case, there was a recast layer at the top and a base material at the bottom, but this arrangement can be rotated. The formation of such lamella with the inverted composition can be achieved by utilizing a nanomanipulator with a 180 degrees needle rotation. One of the nanomanipulators capable of this rotation is called Omniprobe. When sputtering the lamella thus formed, only the secondary transfer of the base material to the adhesive may occur, not the contamination by the electrode material contained in the recast layer, which in turn distorts the information obtained about the chemical composition less than the other way around.

Table 7. The chemical composition analysis in each EDX detail according to Figure 9.

Element	Atomic Fraction (%)	Fit Error (%)
C	3.46	0.67
Si	0.50	0.14
Cr	0.00	0.00
Mn	1.28	0.30
Fe	82.01	19.22
Ni	0.02	0.00
Cu	12.15	2.85
Zn	0.56	0.13
Mo	0.02	0.01

To define the impact of the WEDM process on the crystal lattice of the material, a diffraction mode measurement was carried out in the transmission modes with a beam current of about 13 nA in the base material interface and the recast layer, as depicted in Figure 9. Comparing the diffraction pattern of the base material and the recast layer, it is apparent that the machining of Hardox 400 with WEDM caused a residual stress increase. This resulted in a change in the position of the individual diffraction points. A similar change of the crystal lattice after WEDM was observed in the machining of martensitic steel Huang et al. [9,21–23].

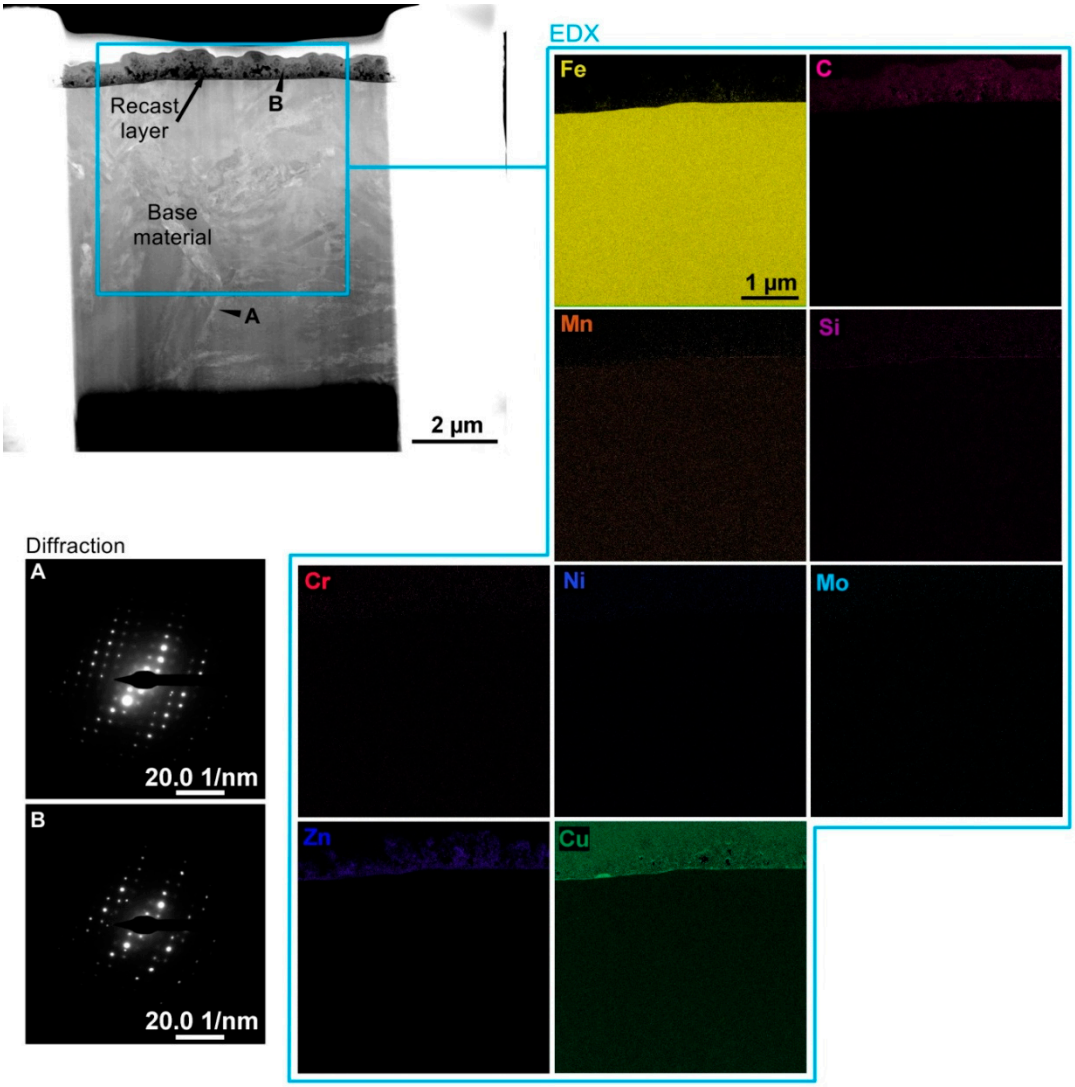

Figure 9. TEM lamella of Hardox 400 steel including the map of individual elements in the examined area of the lamella and a comparison of the diffraction pattern of A—base material and with B—the area near the recast layer.

4. Conclusions

In order to investigate in detail, the impact of WEDM on the machined material, TEM lamella made of the Ti-6Al-4V titanium alloy, AlZn6MgCu aluminum alloy, pure molybdenum, Creusabro 4800 steel, and Hardox 400 steel were manufactured. Based on the analysis of the distribution of individual elements and diffractions, the following conclusions were achieved:

1. Due to WEDM, the concentration of base material elements in the recast layer (Fe, Si, Mn, and Ti) was increased in the AlZn6MgCu aluminum alloy, and copper precipitates were formed in the grain boundary area, with the diffraction pattern showing that there was a slight increase in the residual stress in the recast layer,
2. As a result of the Ti-6Al-4V titanium alloy machining, a strong diffusion from the wire electrode to the material being machined has been demonstrated, an increased concentration of Al, Fe, and O has been monitored in the recast layer. Moreover, from the comparison of the diffraction patterns of the base material and the area of the adhesive, the major amorphization of the crystal structure of the material occurred due to WEDM,

3. In the case of pure molybdenum, the phenomenon of over-diffusion of the elements from the wire electrode, especially copper, into the grain boundary area and the resulting crack was observed, from the diffraction pattern there is an apparent increase in the residual stress in the recast layer,
4. On the Creusabro steel an increased concentration of carbon, phosphorus, sulphur, titanium, and zinc on the surface of the adhesive was found, in the recast layer area of Hardox steel, the base material was mixed with the electrode material, and the local concentration of the base material chemical elements in the recast layer was changed due to WEDM.

In terms of surface topography comparison, the lowest parameters and hence the highest surface quality were achieved with pure molybdenum, and it is clear that higher surface qualities can be achieved with non-ferrous materials. In terms of surface morphology, the individual materials are also very different, both in terms of crater size and frequency.

From the abovementioned conclusions, it is clear that each material is slightly differently affected by the effects of WEDM, and only a detailed research can bring valuable knowledge towards more efficient machining and also prevent the early end of the service life of the produced parts.

Author Contributions: Conceptualization, K.M. and R.Z.; methodology, K.M., T.P. and R.H.; validation, K.M., J.F. and L.B.; formal analysis, R.Z.; investigation, K.M., R.Z., T.P., R.H. and J.F.; resources, J.F. and L.B.; data curation, K.M. and T.P.; writing—original draft preparation, K.M.; writing—review and editing, K.M.; supervision, K.M.; funding acquisition, L.B. and J.F. All authors have read and agreed to the published version of the manuscript.

Funding: The Czech Nano Lab project LM2018110 funded by MEYS CR is gratefully acknowledged for the financial support of the measurements/sample fabrication at CEITEC Nano Research Infrastructure. The article was supported by project no. FEKT-S-17-3934 for the utilization of novel findings in micro and nanotechnologies for complex electronic circuits and sensor applications. This research has been financially supported by the Specific University Research grant of Brno University of Technology, FEKT/STI-J-18-5354. Research described in this paper was also financed by the Czech Ministry of Education in frame of the National Sustainability Program under grant LO1401. For research, the infrastructure of the SIX Center was used. This work was supported through the internal grant provided by the Jan Evangelista Purkyně University in Ústí nad Labem, called SGS (Student Grant Competition), No. 0004/2015, and partly by the Ministry of Education, Youth and Sport of the Czech Republic, the program NPU1, project No. LO1207.

Conflicts of Interest: The authors declare no conflict of interest.

References

1. Vates, U.K. *Wire-EDM Process Parameters and Optimization*; Springer: Berlin, Germany, 2018; ISBN 978-620-2-30578-5.
2. Ranjan, R. *Optimization of Wire Electrical Discharge Machining*; Lap lambert academic publisher: Saarbrücken, Germany, 2016; ISBN 978-3-659-88968-4.
3. McGeough, J.A. *Advanced Methods of Machining*; Springer Science & Business Media: Heidelberg, Germany, 1988; ISBN 0-412-31970-5.
4. Ghodsiyeh, D.; Golshan, A.J.; Shirvanehdeh, A. Review on current research trends in wire electrical discharge machining (WEDM). *Indian J. Sci. Technol.* **2013**, *6*, 4128–4140. [CrossRef]
5. Klink, A. Wire electro discharge trueing and dressing of fine grinding wheels. *CIRP Ann.* **2010**, *59*, 235–238. [CrossRef]
6. Huang, C.A.; Tu, G.C.; Yao, H.T.; Kuo, H.H. Characteristics of the rough-cut surface of quenched and tempered martensitic stainless steel using wire electrical discharge machining. *Metal. Mater. Trans. A* **2004**, *35*, 1351–1357. [CrossRef]
7. Klocke, F.; Hensgen, L.; Klink, A.; Ehle, L.; Schwedt, A. Structure and composition of the white layer in the wire-EDM process. *Procedia CIRP* **2016**, *42*, 673–678. [CrossRef]
8. Zhang, C. Effect of wire electrical discharge machining (WEDM) parameters on surface integrity of nanocomposite ceramics. *Ceram. Int.* **2014**, *40*, 9657–9662. [CrossRef]
9. Huang, C.A.; Hsu, F.Y.; Yao, S.J. Microstructure analysis of the martensitic stainless steel surface fine-cut by the wire electrode discharge machining (WEDM). *Mater. Sci. Eng. A* **2004**, *371*, 119–126. [CrossRef]
10. Murray, J.W.; Fay, M.W.; Kunieda, M.; Clare, A.T. TEM study on the electrical discharge machined surface of single-crystal silicon. *J. Mater. Process.Technol.* **2013**, *213*, 801–809. [CrossRef]

11. Jose, J.V.; Shunmugam, M.S. Investigation into white layer formed on wire electrical discharge machined Ti6Al4V surface. *Int. J. Mach. Mach. Mater.* **2009**, *6*, 234–249. [CrossRef]
12. Liu, J.F.; Guo, Y.B.; Butler, T.M.; Weaver, M.L. Crystallography, compositions, and properties of white layer by wire electrical discharge machining of nitinol shape memory alloy. *Mater. Des.* **2016**, *109*, 1–9. [CrossRef]
13. Sanchez, J.A.; Plaza, S.; Lopez de Lacalle, L.N.; Lamikiz, A. Computer simulation of wire-EDM taper-cutting. *Int. J. Computer Integr. Manuf.* **2006**, *19*, 727–735. [CrossRef]
14. Punturat, J.; Tangwarodomnukun, V.; Dumkum, C. Surface characteristics and damage of monocrystalline silicon induced by wire-EDM. *Appl. Surf. Sci.* **2014**, *320*, 83–92. [CrossRef]
15. Chaudhari, R.; Vora, J.J.; Patel, V.; López de Lacalle, L.N.; Parikh, D.M. Surface Analysis of Wire-Electrical-Discharge-Machining-Processed Shape-Memory Alloys. *Materials* **2020**, *13*, 530. [CrossRef] [PubMed]
16. Jiang, X.J.; Whitehouse, D.J. Technological shifts in surface metrology. *CIRP Ann. Manuf. Technol.* **2012**, *61*, 815–836. [CrossRef]
17. *Geometrical Product Specifications (GPS)—Surface texture: Areal—Part 2: Terms, Definitions and Surface Texture Parameters*; ISO 25178-2 (2012); International Organization for Standardization: Geneva, Switzerland, 2012.
18. *Geometrical Product Specifications (GPS)—Surface Texture: Profile Method—Rules and Procedures for the Assessment of Surface Texture*; ISO 4288: 1996; International Organization for Standardization: Geneva, Switzerland, 1996.
19. Ikram, A.; Mufti, N.A.; Saleem, M.Q.; Khan, A.R. Parametric optimization for surface roughness, kerf and MRR in wire electrical discharge machining (WEDM) using Taguchi design of experiment. *J. Mech. Sci. Technol.* **2013**, *27*, 2133–2141. [CrossRef]
20. Majumder, H.; Maity, K. Prediction and optimization of surface roughness and micro-hardness using grnn and MOORA-fuzzy-a MCDM approach for nitinol in WEDM. *Measurement* **2018**, *118*, 1–13. [CrossRef]
21. Mouralova, K.; Kovar, J.; Klakurkova, L.; Prokes, T.; Horynova, M. Comparison of morphology and topography of surfaces of WEDM machined structural materials. *Measurement* **2017**, *104*, 12–20. [CrossRef]
22. Mouralova, K.; Kovar, J.; Klakurkova, L.; Bednar, J.; Benes, L.; Zahradnicek, R. Analysis of surface morphology and topography of pure aluminium machined using WEDM. *Measurement* **2018**, *114*, 169–176. [CrossRef]
23. Mouralova, K.; Benes, L.; Zahradnicek, R.; Bednar, J.; Hrabec, P.; Prokes, T.; Hrdy, R. Analysis of cut orientation through half-finished product using WEDM. *Mater. Manuf. Processes* **2019**, *34*, 70–82. [CrossRef]

© 2020 by the authors. Licensee MDPI, Basel, Switzerland. This article is an open access article distributed under the terms and conditions of the Creative Commons Attribution (CC BY) license (http://creativecommons.org/licenses/by/4.0/).